Colloid Polym Sci (2002) 280: 591–598
DOI 10.1007/s00396-001-0646-z

ORIGINAL CONTRIBUTION

M. Krumova
A. Flores
F.J. Baltá Calleja
S. Fakirov

Elastic properties of oriented polymers, blends and reinforced composites using the microindentation technique

Received: 15 October 2001
Accepted: 11 December 2001
Published online: 14 May 2002
© Springer-Verlag 2002

M. Krumova · A. Flores
F.J. Baltá Calleja (✉)
Instituto de Estructura de la Materia,
CSIC, Serrano 119, 28006 Madrid, Spain

S. Fakirov
Institut für Verbundwerkstoffe GmbH,
Universität Kaiserslautern, Postfach 3049,
67653 Kaiserslautern, Germany

Permanent address: S. Fakirov
Laboratory of Structure and Properties
of Polymers, University of Sofia,
1126 Sofia, Bulgaria

Abstract The elastic behaviour of poly(ethylene terephthalate) (PET) and nylon 6 (PA6), their blends (1:1 by weight) and microfibrillar-reinforced composites of the previously mentioned homopolymers has been investigated by means of load–displacement analysis from indentation experiments. The dependence of the elastic modulus of the homopolymers upon the degree of crystallinity and the crystal size, as derived from indentation experiments, is discussed. A linear correlation between the elastic modulus anisotropy and the microindentation hardness anisotropy values is also found to apply for the oriented materials. The results reveal that the indentation modulus values of the PET/PA6 blends follow the parallel additivity model of the individual components. The use of the additivity law is also shown to provide a value, otherwise not accessible from direct measurements, of the modulus of the microfibrils within the microfibrillar-reinforced composites.

Keywords Poly(ethylene terephthalate) · Nylon 6 · Blends · Microfibrillar-reinforced composites · Microindentation hardness

Introduction

In the last few years a number of studies concerning the elastic properties of several materials using indentation techniques have been reported [1, 2, 3, 4, 5, 6, 7, 8]. The use of modern ultramicrohardness devices enables continuous load–displacement monitoring as the indenter is driven into and out of the surface of the samples investigated [1, 2]. The slope of the unloading curves is regarded as a measure of the elastic properties of the materials studied. Several methods have been proposed for the calculation of values of Young's modulus from indentation depth-sensing curves [1, 2, 3]. The majority of the previously cited studies deal with the elastic modulus of inorganic materials: metals, ceramics or oxide films. Studies on organic materials are exclusively devoted to neat polymers [3, 4, 7, 8]. The influence of polymer microstructure (crystallinity, crystal size, etc.) on the elastic modulus of poly(ethylene terephthalate) (PET), as derived from indentation experiments, has been the subject of a recent report [9]. The aim of the present study is to extend the previously mentioned investigations to other oriented polymers, polymer blends and composites.

A new type of polymer composites, namely microfibrillar-reinforced composites (MFCs), has been developed lately [10, 11, 12]. The processing of MFCs is substantially different from conventional macrocomposites. In MFCs, both components are initially blended and are subsequently drawn. During the drawing process, microfibrils are created, which act as a reinforcement to the polymer matrix [10]. Additional annealing of the composite above the melting temperature of the lower-melting component produces the isotropization of the polymer matrix, while the oriented microfibrillar structure is preserved. Furthermore, during the annealing

treatment, a copolymer phase is formed at the interfaces of the microfibrils, thus, ensuring good adhesion between the microfibrils and the surrounding matrix [13].

In a preceding study, the structure development during the different processing stages of PET/nylon 6 (PA6) MFCs was followed by X-ray scattering, scanning electron microscopy (SEM) and microhardness techniques [13]. The PET microfibrils were shown to notably enhance the mechanical properties of the PA6 matrix. In addition, the study highlighted the capability of the microhardness technique, using the additivity relationship of individual components, to reveal the micromechanical properties of the microfibrils that are, otherwise, not accessible from direct measurements.

In the present work we complement the previous studies by investigating the elastic modulus derived from microindentation, E, in oriented polymer systems (PET, PA6) in relation to the microstructure, whether the additivity relation holds for the indentation E modulus of polymer blends (PET/PA6) and the elastic properties of the microfibrils within the microfibrillar reinforced composites.

Experimental

Materials

The polymers used were PET (Goodyear Merge 1934F, $M_n = 23{,}400$ g/mol) and PA6 (Allied Signal Capron 8200, $M_n = 20{,}600$ g/mol). These polymers were ground to a particle size of less than 0.4 mm (after cooling in liquid nitrogen) and were subsequently mixed in the solid state (1:1 wt/wt). Homogeneous quenched films (on a microscopic scale) of the blend and of the respective homopolymers, of thickness 0.10-0.13 mm and width 4-5 mm, were prepared according to the procedure described in Ref. [13]. X-ray scattering and differential scanning calorimetry (DSC) measurements of all the quenched samples revealed an amorphous isotropic structure for PET, while the PA6 and PET/PA6 samples were shown to develop partial crystallinity.

Quenched samples of both, homopolymers and blends, were subjected to a drawing process as described in Ref. [13], followed by annealing in a vacuum with fixed ends at 220 or 240 °C for 5 or 25 h. The sample preparation conditions are given in Table 1. The structure and morphology of the samples were characterized by means of X-ray diffraction, DSC and SEM measurements [13]. The blends subjected to the highest annealing temperature (B-D-3 and B-D-4) present a MFC structure [13].

Technique and calculation procedure

For the indentation experiments with continuous load–displacement monitoring during loading and unloading, an ultramicrohardness tester (Shimadzu DUH-202) was used. The measurements were performed at room temperature with a Vickers indenter, i.e. a square-based diamond pyramid.

A peak load of 147 mN was reached at a loading rate of 13.2 mN/s. After a holding time of 6 s, the load was released at the same constant velocity as in the loading cycle. For each E value five to ten measurements were averaged.

As an example, a typical load–displacement curve for an oriented PET sample is shown in Fig. 1. The reduced modulus, E^*, also known as the indentation modulus [14], was derived by the procedure proposed in Ref. [2], according to the equation

$$E^* = \left(\frac{\pi}{A}\right)^{1/2} \frac{S}{2}, \tag{1}$$

where $S = \partial P/\partial h$ is the initial unloading stiffness (Fig. 1) and $A = 24.5 h_c^2$ is the projected area of contact at maximum load between the indenter and the sample. E is related to E^* through the equation

$$E = E^*\left(1 - \nu^2\right), \tag{2}$$

where ν is the Poisson ratio for the material tested. We have assumed $\nu = 0.3$ for the amorphous samples and $\nu = 0.35$ for the semicrystalline ones [15].

The contact depth, h_c, is derived using the following equation:

$$h_c = h_p + (1 - \varepsilon)(h_{max} - h_p), \tag{3}$$

Table 1. Sample preparation conditions

Sample designation	Composition: poly (ethylene terephthalate)/ nylon 6 (wt/wt)	Zone drawing		Annealing in vacuum with fixed ends	
		Temperature (°C)	Draw ratio	T_a (°C)	t_a (h)
PET-Q	100/0	–	–	–	–
PET-D	100/0	85	4.0	–	–
PET-D-1	100/0	85	4.0	220	5
PET-D-2	100/0	85	4.0	220	25
PET-D-4	100/0	85	4.0	240	25
PA-Q	0/100	–	–	–	–
PA-D	0/100	180	3.8	–	–
PA-D-1	0/100	180	3.8	220	5
PA-D-2	0/100	180	3.8	220	25
B-Q	50/50	–	–	–	–
B-D	50/50	180	4.2	–	–
B-D-1	50/50	180	4.2	220	5
B-D-2	50/50	180	4.2	220	25
B-D-3	50/50	180	4.2	240	5
B-D-4	50/50	180	4.2	240	25

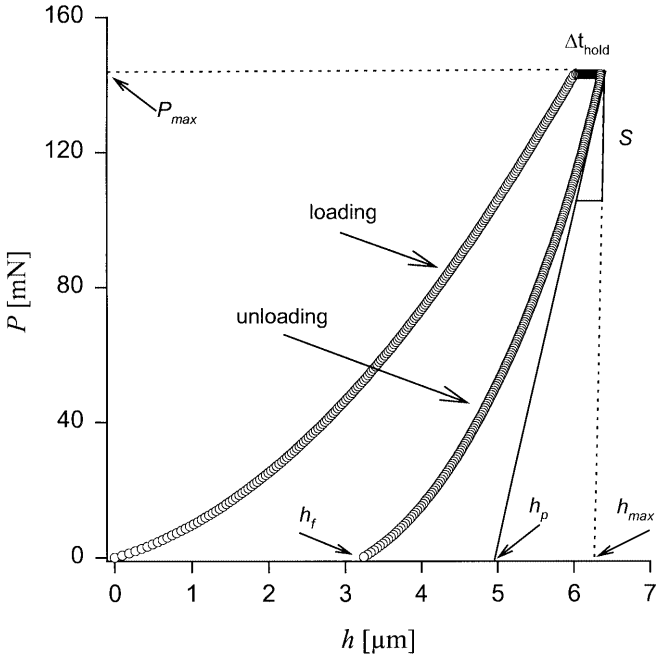

Fig. 1. Load versus displacement recorded during an indentation cycle on oriented poly(ethylene terephthalate) (*PET*)

where h_p is calculated from the intercept of the initial unloading slope with the displacement axis (as shown in Fig. 1), h_{max} is the maximum displacement reached by the indenter and ϵ is a constant dependent on the indenter geometry. In our case, an ϵ value of 0.72 was chosen, which corresponds to a conical geometry. Furthermore, the method uses a power-law relationship to describe the unloading curves:

$$P = \alpha(h - h_f)^n, \tag{4}$$

where P is the load at a given penetration depth h, and the constants α, h_f and n are determined by a least-squares fitting procedure. The initial unloading stiffness, S, was found by analytically differentiating Eq. (4) and evaluating the derivative at the maximum load and displacement.

To minimize the error in the determination of the true zero of indentation depth, the experimental loading curve was fitted to a power-law function of the type

$$P = m(h - h_0)^{n'}, \tag{5}$$

where m is a material constant, n' is the index of the deformation and h_0 is the true zero point.

Results and discussion

The values of E^* obtained according to Eq. (1), the elastic modulus values calculated using Eq. (2) and the values of Young's modulus, E_T, derived from the stress–strain curves of previous tensile measurements [13] are shown in Table 2. The latter E_T values were determined with an error of $\pm 5\%$. The evolution of E^* for blend samples prepared at various stages of the MFC processing (Table 1) is shown in Fig. 2; values for the homopolymers are also included for comparison. In all cases, there is a tendency for the E^* values to increase after the various processing stages, i.e., orientation and increase in temperature and annealing time. This result is a consequence of the specific structure developed at each processing stage. An attempt is made later to evaluate independently the influence of some of the morphological parameters upon E^*.

Influence of microstructure on the elastic modulus

Degree of crystallinity

In addition to the elastic modulus, the degree of crystallinity, w_c, from DSC and the crystal size of PA6, D_{200},

Table 2. Reduced modulus, E^*, derived from microindentation measurements, elastic modulus, $E = E^*(1\text{-}\nu^2)$, Young's modulus, E_T, from tensile testing, degree of crystallinity, w_c, crystal size of nylon 6, D_{200}, microhardness, H, and microindentation anisotropy, ΔH

Sample	E^* (GPa)	E (GPa)	E_T (GPa)	w_c (differential scanning calorimetry)		D_{200} (nm)	H (MPa)	ΔH (%)
PET-Q	3.35 ± 0.07	3.05 ± 0.06	1.1	0.04			134	0
PET-D	2.6 ± 0.1	2.30 ± 0.07	9.4	0.10			147	34.0
PET-D-1	3.43 ± 0.08	3.01 ± 0.06	10.6	0.44			194	25.3
PET-D-2	4.04 ± 0.08	3.54 ± 0.06	11.4	0.49			216	22.4
PET-D-4	4.4 ± 0.1	3.8 ± 0.1	9.5	0.48			240	15.1
PA-Q	1.76 ± 0.04	1.54 ± 0.03	0.2	0.28		3.3	117	0
PA-D	2.5 ± 0.1	2.2 ± 0.1	4.5	0.32		4.1	126	10.8
PA-D-1	3.2 ± 0.1	2.8 ± 0.1	4.8	0.35		9.7	133	7.3
PA-D-2	2.87 ± 0.04	2.73 ± 0.03	2.7	0.31		10.6	150	5.0
				PET	PA6			
B-Q	2.8 ± 0.1	2.47 ± 0.08	–	0.17	0.25	–	131	0
B-D	3.1 ± 0.1	2.73 ± 0.08	8.8	0.39	0.29	3.7	152	27.0
B-D-1	3.32 ± 0.05	2.91 ± 0.01	9.3	0.46	0.38	8.3	170	19.0
B-D-2	3.4 ± 0.1	3.0 ± 0.1	9.8	0.48	0.36	8.6	172	20.7
B-D-3	4.1 ± 0.1	3.6 ± 0.1	7.8	0.53	0.19	12.2	175	6.5
B-D-4	4.2 ± 0.1	3.6 ± 0.1	8.6	0.75	0		177	4.3

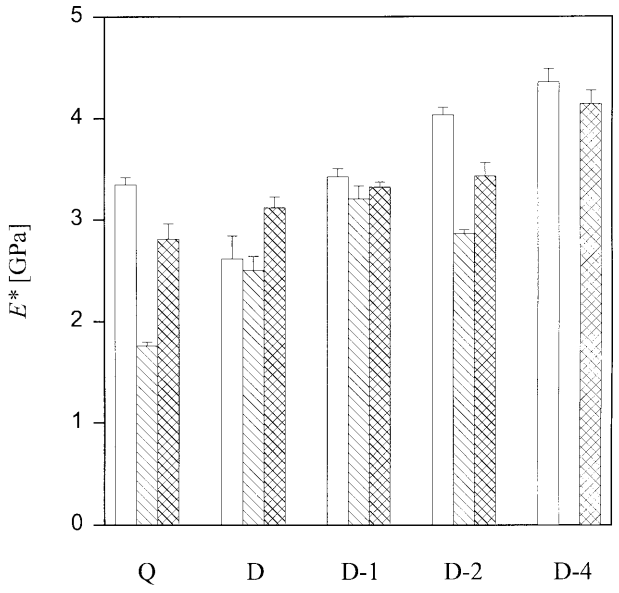

Fig. 2. E^* values after the various stages for the microfibrillar-reinforced composite (*MFC*) processing (see Table 1). *First column*: neat PET; *second column*: neat nylon 6 (*PA6*); *third column*: blend

from wide-angle X-ray scattering, as taken from Ref. [13], are collected in Table 2.

The variation of E^* as a function of w_c^{PET} for the oriented homopolymer PET is presented in Fig. 3. The E^* values measured on other oriented PET samples with the same draw ratio are also included [9]. From the extrapolation of the linear dependence, an E^* value for the amorphous oriented PET (drawn at $\lambda = 4$) of 2.3 GPa can be estimated. This value is slightly lower, though it lies within the range of E^* recently measured on other amorphous oriented PET samples [9] (Fig. 3).

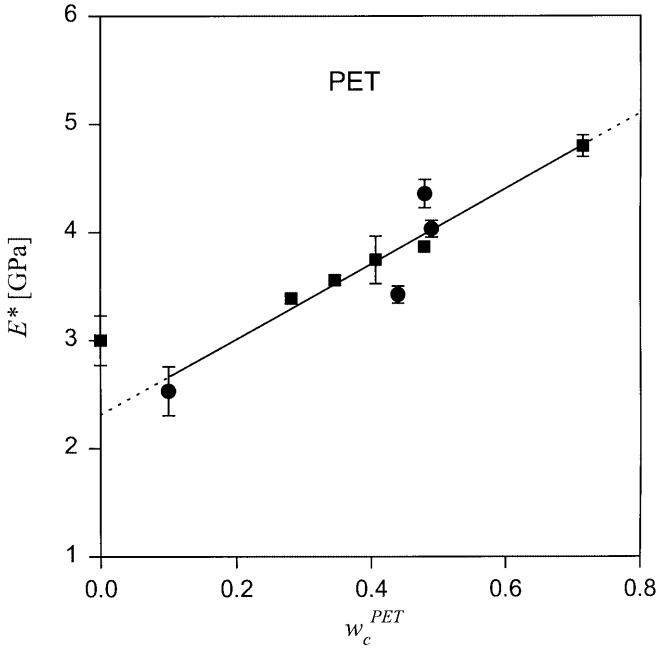

Fig. 3. Plot of E^* versus the degree of crystallinity for oriented PET. The *squares* are taken from Ref. [9]

Crystal size

In contrast to PET, the w_c values of PA6 remain practically constant (around 30%) irrespective of the preparation conditions. However, PA6 shows a clear increase in the crystal size (Table 2) upon both drawing and further thermal treatment (Table 1). In our preceding study we showed that the microhardness of neat PA6 decreases linearly with the reciprocal of the crystal size ($1/D_{200}$). Therefore, the linear correlation between E^* and H for PA6 (see next section) supports the E^* dependence upon the crystal size illustrated in Fig. 4. The extrapolation of the straight line for $1/D_{200} = 0$ yields an E^* value of 3.8 GPa. This value would correspond to a 30% crystallinity system consisting of infinitely large crystals. Hence, an ideal fully crystalline PA6 made of infinite large crystals should have a maximum E^* value of about $E^*_\infty = 12$ GPa. This value is analogous to the ideal microhardness value of infinitely thick crystals [16].

E–H correlation

The values of the microhardness, H, and the indentation anisotropy, ΔH, obtained in a preceding study [13] are

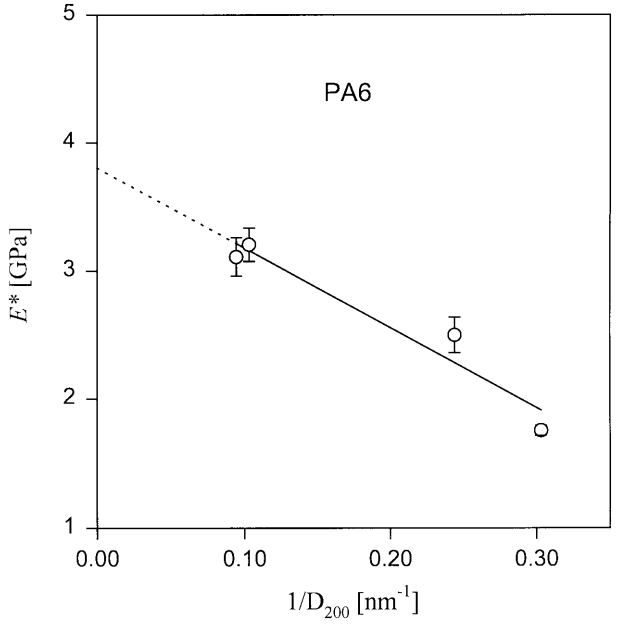

Fig. 4. Plot of E^* versus reciprocal crystal size, $1/D_{200}$, for PA6

also included in Table 2. Microindentation hardness measurements were performed using a square-based diamond. The values of H and ΔH were derived from the diagonal of the residual impression after load release. Owing to sample orientation, two different diagonal values, $d_{\|}$ and $d_{\perp}$, the impression diagonals parallel and perpendicular to the draw axis, respectively, emerged. Indentation anisotropy is defined as [16]

$$\Delta H = 1 - (d_{\|}/d_{\perp})^2. \quad (6)$$

The relation between the E values, evaluated from microindentation measurements, and the H values taken from Table 2 is depicted in Fig. 5. It is known that the E/H ratio offers a convenient measure of the plastic-to-elastic contribution to the total indentation depth [17]. A first-order regression fit to the E–H values gives different slopes for the homopolymers, the blends and the composites. The slope for the oriented blends ($E/H = 17$) lies between the slopes of the PET ($E/H = 16$) and PA6 ($E/H = 19$) homopolymers. In other words, PA6 exhibits a markedly plastic character compared to PET. It is noteworthy that the microfibrillar composites present, for a similar microhardness value as that of the blends, the highest E values (largest E/H ratio).

Anisotropy of elastic behaviour

The E values for oriented samples, as derived from indentation measurements, appear to be significantly lower than the E_T values obtained from tensile tests (Table 2). This result is a consequence of the different loading directions during both kinds of testing. While in the tensile tests the load was applied along the draw direction, in the indentation tests the load was perpendicular to this direction. It is well known that oriented polymers exhibit a mechanical anisotropy owing to the different cohesive forces along and across the chain direction [18].

On the other hand, the results show that the E values for the quenched isotropic homopolymers are larger than the corresponding E_T values (Table 2). This is a well-known observation, which has been explained in terms of the hydrostatic component of stress which enhances the E compressive values in isotropic polymers [19].

As E and E_T reflect the elastic properties perpendicular and parallel to the draw direction, respectively, we attempted to examine the possible correlation between the E_T/E ratio and the microhardness anisotropy, ΔH. Indeed, Fig. 6 shows an apparent linear dependence for the PET homopolymer (continuous line), as well as for the blends and composites (dotted line). It seems that oriented PA6 follows the trend of PET (the deviation of the data point for $E_T/E = 1$ is probably due to the uncertainty in the measurement of the E_T value). The plot in Fig. 6 could be relevant from a practical point of view, as it may allow the rapid evaluation of the elastic behaviour anisotropy in oriented polymers using the microhardness technique. However, one may expect that the E_T/E–ΔH slope in Fig. 6 could change with the strain rate used in the tensile experiment [20].

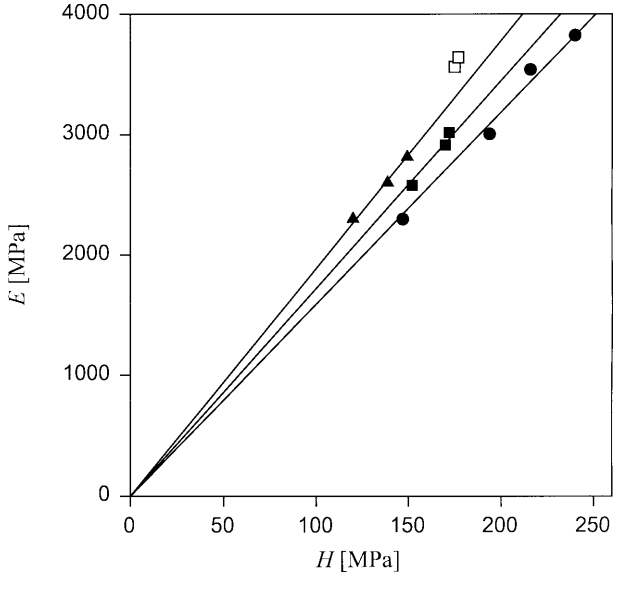

Fig. 5. Plot of E versus H for oriented PET (*circles*), PA6 (*triangles*), blends (*filled squares*) and composites (*open squares*)

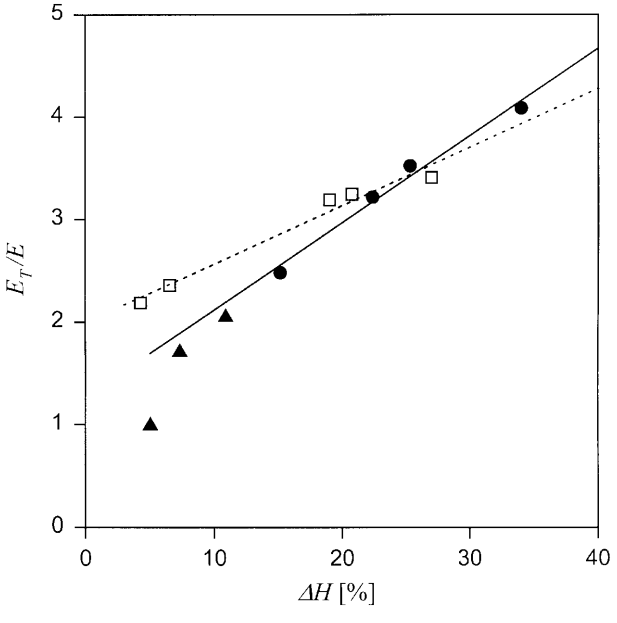

Fig. 6. Correlation between E_T/E and microindentation anisotropy, ΔH, in oriented PET (*circles*), PA6 (*triangles*) and blends and composites (*squares*)

Additivity law for the elastic modulus derived from microindentation

Mechanical properties of complex polymer systems frequently follow additive relationships with respect to the constituent components. Several theoretical approximations have been developed to predict the modulus of two-phase blends [18]. The parallel and the series models present the two simplest lines of approach. The former case assumes that each component undergoes the same strain, with the stresses being summed up:

$$E = \varphi_1 E_1 + \varphi_2 E_2. \tag{7}$$

The latter case assumes a summation of strains for each component subjected to the same stress:

$$\frac{1}{E} = \frac{\varphi_1}{E_1} + \frac{\varphi_2}{E_2}. \tag{8}$$

In addition, there are other models which take into account the influence of the adhesion and the morphology of the components on the elastic properties of the blends and composites [18, 21]. Scanning electron micrographs of MFC and drawn blends reveal a nearly perfect alignment of the microfibrils in the draw direction [13] and good adhesion between the microfibrils and the matrix in the former. Thus, we also applied the Halpin–Tsai model, for which the transverse modulus of the blend is described in terms of the constituents through [21]

$$E = E_m \frac{1 + \xi\eta V_f}{1 - \eta V_f}, \tag{9}$$

$$\eta = \frac{E_f/E_m - 1}{E_f/E_m + \xi}, \tag{10}$$

where E_m and E_f are the elastic moduli of the matrix and the reinforcing fibres (PA6 and PET, respectively), V_f is the volume fraction of the fibre, being equal to φ_1 in Eqs. (7) and (8) and ξ is a measure of the degree of interfacial adhesion between fibre and matrix and of other morphological details.

Blends

The experimental E^* values and the E^* values calculated according to the previously described models for the blends studied ($\varphi_1 = \varphi_2 = 0.5$) are summarized in Table 3. To derive the calculated data, the E^* values of the components of the blend were approximated to those of the respective homopolymer samples (Table 2). In addition, we assumed a perfect interfacial adhesion in Eqs. (9) and (10) ($\xi = 2$). To take into account the differences in w_c and D_{200} between the blend components and the homopolymers, we derived E^* from the plots in Figs. 3 and 4 when appropriate. The results obtained are collected in Fig. 7. Except for the first sample (B-Q), the three models fit reasonably well to the experimental values. This result could be a consequence of the similar mechanical properties of the matrix and the fibres, in contrast to other common composites (glass-fibre reinforced epoxy resins, etc.) where the difference in the mechanical properties of the constituents is large.

Table 3. Measured E^* values and E^* values calculated according to Eqs. (7), (8) and (9)

Sample	E^*_{meas} (GPa)	$E^*_{parallel}$ (GPa)	E^*_{series} (GPa)	$E^*_{Halpin–Tsai}$ (GPa)
B-Q	2.81 ± 0.15	2.56	2.31	2.45
B-D	3.12 ± 0.11	3.09	2.98	3.05
B-D-1	3.32 ± 0.05	3.32	3.31	3.32
B-D-2	3.44 ± 0.13	3.45	3.35	3.42

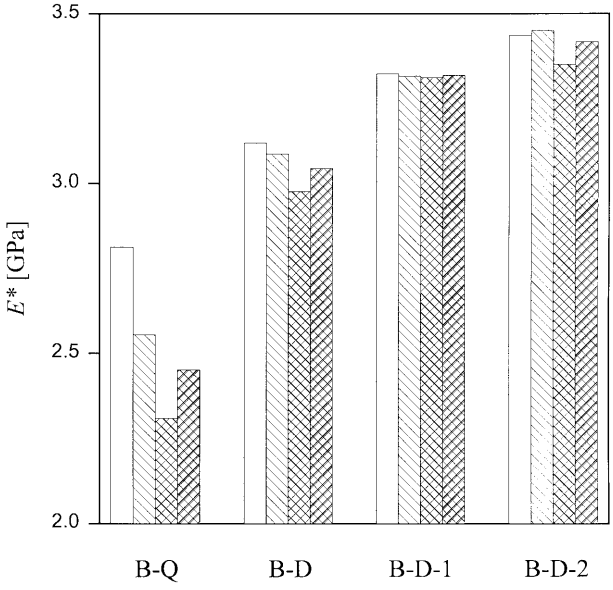

Fig. 7. Experimental E^* values for the PET/PA6 blends (*first column*) and calculated E^* values according to the parallel model (*second column*), the series model (*third column*) and the Halpin–Tsai equations (*fourth column*)

For the isotropic blend B-Q, the calculated values are shown to be smaller than the measured ones. This deviation is a result of the different degree of crystallinity of the PET component within the blend (about 17%) with respect to the w_c^{PET} value of the corresponding unoriented homopolymer (4%). In this case, the previous correction could not be performed because the E–w_c^{PET} relationship of Fig. 3 refers to oriented systems.

The small difference between the parallel and the series model could be related to the specific morphology of the microfibrils, which have been shown to form an

interpenetrating mesh along the orientation direction [13]. During an indentation cycle, the randomly interpenetrated microfibrillar mesh is plastically deformed under the influence of a compressive force, presumably yielding a complex series–parallel mechanical response.

Microfibrillar-reinforced composites

Reinforcing microfibrils in the MFCs samples (B-D-3 and B-D-4) are formed during the drawing process of the PET/PA6 blends [11, 12]. Since the direct evaluation of the elastic modulus of the microfibrils is not feasible, as they are not available as separate entities, the microindentation technique offers a possible route for the evaluation of their elastic properties.

In the preceding section, we showed that E^* of the blends can be calculated by means of various additive models of the elastic moduli of the individual components. In what follows, let us use the simplest model, i.e., the parallel model. This behaviour is analogous to the microhardness additivity law for polymer blends [13, 16, 22]; hence, Eq. (7) would describe the E^* values for the different components of the MFC sample treated at the highest annealing temperature for the longest time (sample B-D-4). The morphology of the microfibrillar composite can be approximated by a three-phase system: an amorphous PA6 matrix; an amorphous PET/PA6 "copolymer matrix" which develops owing to the chemical transreactions taking place between the PET and the PA6 molecular segments [23]; and almost fully crystalline microfibrils. Thus, we can rewrite Eq. (7) as follows:

$$E^*_{\mathrm{MFC}} = 0.5(E^{*\mathrm{PA}}_{\alpha} + (1 - w_{\mathrm{c}}^{\mathrm{PET}})E^{*\mathrm{PET}}_{\alpha} + w_{\mathrm{c}}^{\mathrm{PET}}E^{*\mathrm{PET}}_{\mathrm{f}}), \tag{11}$$

where ${w_{\mathrm{c}}}^{\mathrm{PET}} = 0.75$ (Table 2), ${E^*}_{\mathrm{MFC}}$ denotes the experimental reduced elastic modulus of the composite (${E^*}_{\mathrm{MFC}} = 4.2$ GPa), $E^{*\mathrm{PA}}_{\alpha}$ refers to the reduced modulus of the PA6 amorphous matrix, $E^{*\mathrm{PET}}_{\alpha}$corresponds to the modulus of amorphous PET ($E^{*\mathrm{PET}}_{\alpha} = 2.3$ GPa)(Fig. 3) and $E^{*\mathrm{PET}}_{\mathrm{f}}$ is the elastic modulus of the microfibrils. Equation (11) assumes an additivity law for the microhardness of the PET/PA6 copolymer amorphous domains. Let us now estimate the $E^{*\mathrm{PA}}_{\alpha}$value from the E–H dependence shown in Fig. 5. It has been shown that the hardness of an amorphous PA6 sample is $H^{*\mathrm{PA}}_{\alpha} \approx 50$ MPa [13]. This hardness value would yield a corresponding modulus value of approximately $E^{*\mathrm{PA}}_{\alpha} = 1.08$ GPa (Fig. 5). Using Eq. (11) with $E^{*\mathrm{PA}}_{\alpha} = 1.08$ GPa together with the previously mentioned values of the modulus for the different components of the microfibrillar composite, a value of $E^{*\mathrm{PET}}_{\alpha} = 8.9$ GPa is derived. This result is in good agreement with the high H values and reflects the high degree of crystallinity of the microfibrils reported in our preceding study [13].

Conclusions

1. The microindentation technique has been successfully applied for the evaluation of the elastic properties of PET and PA6 neat polymers, their blends and composite-like structures of these materials.
2. Values of E^* of oriented PET samples are shown to be largely influenced by the degree of crystallinity within the samples.
3. A clear dependence of E^* on the crystal size, D_{200}, for PA6 samples with similar degree of crystallinity has been found.
4. A correlation between modulus anisotropy and microhardness anisotropy in the PET- and PA6-based oriented polymers has been derived.
5. The indentation elastic modulus of PET/PA6 blends is shown, for the first time, to follow an additive relationship of the individual components.
6. The use of the E^* additivity law in MFCs permits the evaluation of the modulus of the microfibrils, otherwise not accessible from direct measurements.

Acknowledgements M.K. and A.F. greatly appreciate the fellowship "Programa Cátedra" of the Foundation BBV, Spain, and the postdoctoral grant of the Comunidad Autónoma de Madrid, respectively. We gratefully acknowledge MCYT, Spain (grant BFM2000-1474), for the support of this work. S.F. also acknowledges the support of the German Science Foundation (DFG-FR 675/21–2) and expresses his warmest thanks to the Alexander von Humboldt Foundation for the "Humboldt Research Award".

References

1. Doerner MF, Nix WD (1986) J Mater Res 1:601
2. Oliver WC, Pharr GM (1992) J Mater Res 7:1564
3. Ion RH, Pollock HM, Roques-Carnes C (1990) J Mater Sci 25:1444
4. Briscoe BJ, Sebastian KS, Sinha SK (1996) Philos Mag A 74:1159
5. Loubet JL, Georges JM, Marchesini O, Meille G (1984) J Tribol 106:43
6. Heermant C, Dengel D (1996) Materialpruefung 38:9
7. Flores A, Baltá Calleja FJ (1998) Philos Mag A 78:1283
8. Turnbull A, White D (1996) J Mater Sci 31:4189
9. Flores A, Asano T, Baltá Calleja FJ (2001) J Appl Phys 34:6006
10. Evstatiev M, Fakirov S (1992) Polymer 33:877
11. Fakirov S, Evstatiev M, Friedrich K (2000) In: Paul DR, Bucknall DC (eds) Polymer blends, vol 2. Wiley, New York, p 455

12. Evstatiev M, Fakirov S, Friedrich K (2000) In: Cunha AM, Fakirov S (eds) Structure development during polymer processing. Kluwer, Dordrecht, p 311
13. Krumova M, Fakirov S, Baltá Calleja FJ, Evstatiev M (1998) J Mater Sci 33:2857
14. DIN (1991) 53:479
15. Birley AW, Haworth B, Batchelor J (1992) Physics of plastics. Oxford University Press, Oxford
16. Baltá Calleja FJ, Fakirov S (2000) Microhardness of polymers. Cambridge University Press, Cambridge
17. Baltá Calleja FJ (1985) Adv Polym Sci 66:117
18. Ward IM, Hadley DW (1993) An introduction to the mechanical properties of solid polymers. Wiley, Chichester
19. Ward IM (1971) J Polym Sci C 32:195
20. Baltá Calleja FJ, Giri L, Ward IM, Cansfield DLM (1995) J Mater Sci 30:1139
21. Halpin JC (1992) Primer on composite materials: analysis. Technomic, Lancaster, Pa
22. Baltá Calleja FJ, Giri L, Ezquerra TA, Fakirov S, Roslaniec Z (1997) J Macromol Sci Phys B 36:655
23. Fakirov S, Denchev Z (1999) In: Fakirov S (ed) Transreactions in condensation polymers. Wiley-VCH, Weinheim, p 319